Multiferroic $CoFe_2O_4$–$BiFeO_3$ core–shell nanofibers and their nanoscale magnetoelectric coupling

Qingfeng Zhu,[a] Ying Xie,[a] and Jing Zhang
Faculty of Materials, Optoelectronics and Physics, Xiangtan University, Xiangtan, Hunan 411105, China

Yuanming Liu
Department of Mechanical Engineering, University of Washington, Seattle, Washington 98195

Qingfeng Zhan
Key Laboratory of Magnetic Materials and Devices, Ningbo Institute of Material Technology and Engineering, Chinese Academy of Sciences, Ningbo 315201, China

Hongchen Miao
State Key Lab for Turbulence and Complex Systems, College of Engineering, Peking University, Beijing 100871, China

Shuhong Xie[b]
Key Laboratory of Low Dimensional Materials and Application Technology of Ministry of Education, Xiangtan University, Xiangtan, Hunan 411105, China

(Received 20 September 2013; accepted 24 January 2014)

Multiferroic $CoFe_2O_4$–$BiFeO_3$ (CFO–BFO) core–shell nanofibers were synthesized by coaxial electrospinning. The spinel structure of CFO and perovskite structure of BFO were confirmed by x-ray diffraction and high-resolution transmission electron microscopy. The core–shell configuration of nanofibers was verified by scanning electron microscopy and transmission electron microscopy images. The macroscopic ferromagnetic property of core–shell nanofibers was demonstrated by magnetic hysteresis loop. The local magnetoelectric (ME) coupling was confirmed by using dual frequency piezoresponse force microscopy (PFM) under an external magnetic field, showing magnetically induced evolution of piezoresponse and domain structure. The ferroelectric characteristics are demonstrated by the switching spectroscopy PFM. From PFM hysteresis and butterfly loops, it is observed that the piezoresponse amplitude is reduced while coercive voltage increased under external in-plane magnetic field, induced through the mechanical interactions between magnetostrictive CFO and piezoelectric BFO, from which the lateral ME coupling can be estimated quantitatively. The nanofibers thus can find a variety of applications as a one-dimensional multiferroic material.

I. INTRODUCTION

Multiferroic materials possess two or more types of ferroic orderings and special magnetoelectric (ME) coupling,[1–3] which are not only appealing scientifically, but also promising for a wide range of applications.[4,5] In particular, ME coupling makes it possible to manipulate the electrical state of a multiferroic material through a magnetic field[6,7] or vice versa,[8–11] and thus enables it to control information processing based on electron spin state. However, the ME coupling in single-phase multiferroics is usually extremely small,[12] and to enhance the ME coupling for practical applications, hybrid multiferroic composites consisting of ferroelectric and ferromagnetic phases have been widely explored,[13,14] wherein the ME effect is induced through mechanical interactions arising from magnetostrictive and piezoelectric effects in individual phases.[3]

Low-dimensional multiferroic materials have attracted much attention recently, as they offer much tighter coupling between ferroelectric and ferromagnetic phases, and provide additional degrees of freedom in controlling the size, interface, and epitaxial strain to further enhance the ME coupling. Among them, nanofibers can not only reveal interesting one-dimensional multiferroicity at nanoscale, but could also enable novel ME devices, such as one-dimensional ME probe with nanometer resolution.[15] Furthermore, recent theoretical analysis indicates that composite multiferroic nanofibers exhibit ME responses by orders of magnitude higher than that of thin films with similar compositions,[16] owing to their substantially relaxed substrate constraint. Our recent results on $CoFe_2O_4$–$Pb(Zr_{0.52}Ti_{0.48})O_3$ (CFO–PZT) core–shell nanofibers confirm the theoretical prediction.[17] Compared with PZT, $BiFeO_3$ is lead free and could have larger piezoelectric coefficients,[18] which motivates us to synthesize $CoFe_2O_4$–$BiFeO_3$ multiferroic core–shell nanofibers and explore their ME coupling.

[a]These authors contributed equally to the work.
[b]Address all correspondence to this author.
e-mail: shxie@xtu.edu.cn
DOI: 10.1557/jmr.2014.36

 © Materials Research Society 2014

https://doi.org/10.1557/jmr.2014.36 Published online by Cambridge University Press

In the past decade, many techniques have been developed to fabricate core–shell nanostructures, such as self-assembly,[19] anodic aluminum oxide template,[20] hydrothermal process,[21] chemical vapor deposition,[22] coaxial electrospinning,[23] and so on. Among all these methods, coaxial electrospinning is especially convenient and versatile, and has been adopted to synthesize composite polymer[24,25] and ceramic nanofibers[26–28] widely. Previous work has synthesized $CoFe_2O_4$–$BiFeO_3$ (CFO–BFO) tubular heterostructures and $CoFe_2O_4$/$Bi_{0.97}Ce_{0.03}FeO_3$ coaxial nanotubes by pulsed laser deposition[29] and sol–gel template method,[30] respectively. In this paper, we seek to synthesize $CoFe_2O_4$–$BiFeO_3$ core–shell nanofibers by coaxial electrospinning directly, and examine their morphology, crystalline structure, as well as the multiferroic properties.

II. EXPERIMENT

A. Synthesis of CFO–BFO nanofibers

Multiferroic CFO–BFO core–shell nanofibers were synthesized by sol–gel process and coaxial electrospinning. CFO precursor was synthesized by dissolving appropriate portions of $Fe(C_5H_7O_2)_3$ and $Co(NO_3)_2{\cdot}6H_2O$ in an acetic acid and ethanol hybrid solution with a volume ratio of 1/4, polyvinylpyrrolidone (PVP) with a molecular weight of 1,300,000 was added to the CFO precursor, and stirred continuously to form a 0.6 M homogeneous solution, with the concentration of PVP controlled around 0.04 g/mL. The preparations of BFO precursor with concentration of 0.4 M were described in our early work,[31] in which the concentration of PVP was controlled around 0.06 g/mL. These two solutions were then electrospun using a coaxial spinneret, and the overall setup of coaxial electrospinning is schematically shown in Fig. 1,[23] which consists of three components: a high voltage supplier, a simple collecting system, and two syringe pumps with different diameters and lengths of commercial blunt needles. During the electrospinning process, the syringe loaded with CFO precursor was connected vertically to the needle with 0.7 mm outside diameter as solution for core, and the syringe loaded with BFO precursor was connected horizontally to the needle with 1.28 mm outside diameter as solution for shell. The core solution was driven by a syringe pump (NE-500, New Era Pump Systems, Inc., Farmingdale, NY) at a rate of 0.3 mL/h, whereas the shell solution was driven at a rate of 0.48 mL/h. The needle was connected to a high-voltage power supply (ES40P-5W, Gamma High Voltage, Inc., Ormond Beach, FL), and the distance between the needle tip and the substrate was about 15 cm, with the electric field strength approximately 1.3 kV/cm. The electrospinning temperature was about 20 °C. The electrospun nanofibers were collected to Pt/Ti/SiO_2/Si substrates, dried at 120 °C for 4 h, followed by thermal annealing at 750 °C for 2 h in air.

B. Characterization

The crystalline structure of nanofibers was examined by x-ray diffraction (XRD, Rigaku D/max-rA, Rigaku Inc., Tokyo, Japan) with Cu K_α radiation (λ = 0.15406 nm) and high-resolution transmission electron microscopy (HRTEM). The morphology of CFO–BFO core–shell nanofibers was observed by scanning electron microscopy (SEM, Hitachi S4800, Hitachi Ltd., Tokyo, Japan) and transmission electron microscopy (TEM, JEM-2100, JEOL, Tokyo, Japan). The macroscopic ferromagnetic property of nanofibers was measured by Lakeshore vibrating sample magnetometer (VSM). The ferroelectric and ME coupling properties of nanofibers were examined by piezoresponse force microscopy (PFM) with variable field module (VFM) using an Asylum Research MFP-3D atomic force microscope (AFM) with a procedure described in our earlier paper.[17] Two nanofiber samples (sample 1 and sample 2) were measured to demonstrate the ME coupling of the core shell nanofibers.

III. RESULTS AND DISCUSSION

A. Crystalline structure

The crystalline phases of core–shell nanofibers were examined by XRD, as shown in Fig. 2, where two distinct sets of diffraction peaks are observed, corresponding to perovskite BFO and spinel CFO phases, respectively, and no obvious impurity phases are found in the composite nanofibers. Furthermore, the diffraction peaks of BFO are more broader than that of CFO, which indicates that the grain size of BFO phase is less than that of CFO, and the effective amount of CFO core phase is larger than that of BFO shell phase.

B. Morphology

The SEM, TEM, and HRTEM images of CFO–BFO core–shell nanofibers are shown in Fig. 3. It is observed that the diameter of nanofibers is in the range of 200–600 nm, while the surface is not smooth as CFO–PZT core shell fibers owing to the grain size of PZT nanofiber are much less than that of BFO,[17] as shown in Fig. 3(a). The typical cross-section topography of the nanofibers is shown in Fig. 3(b), where the core–shell structure is evident, and majority interfaces are compact, though small gaps exist at the interfaces between BFO core and CFO shell due to the inhomogeneous shrinkage of ceramic fibers during calcination. The core–shell structure of the nanofiber is further confirmed by TEM image, as seen in Fig. 3(c), where the interface between BFO shell and CFO core is visible. It is estimated that the outer diameter of BFO shell is approximately 400 nm, whereas the diameter of the CFO core is about 260 nm. This is consistent with the different flow rates for BFO and CFO during electrospinning process

https://doi.org/10.1557/jmr.2014.36 Published online by Cambridge University Press

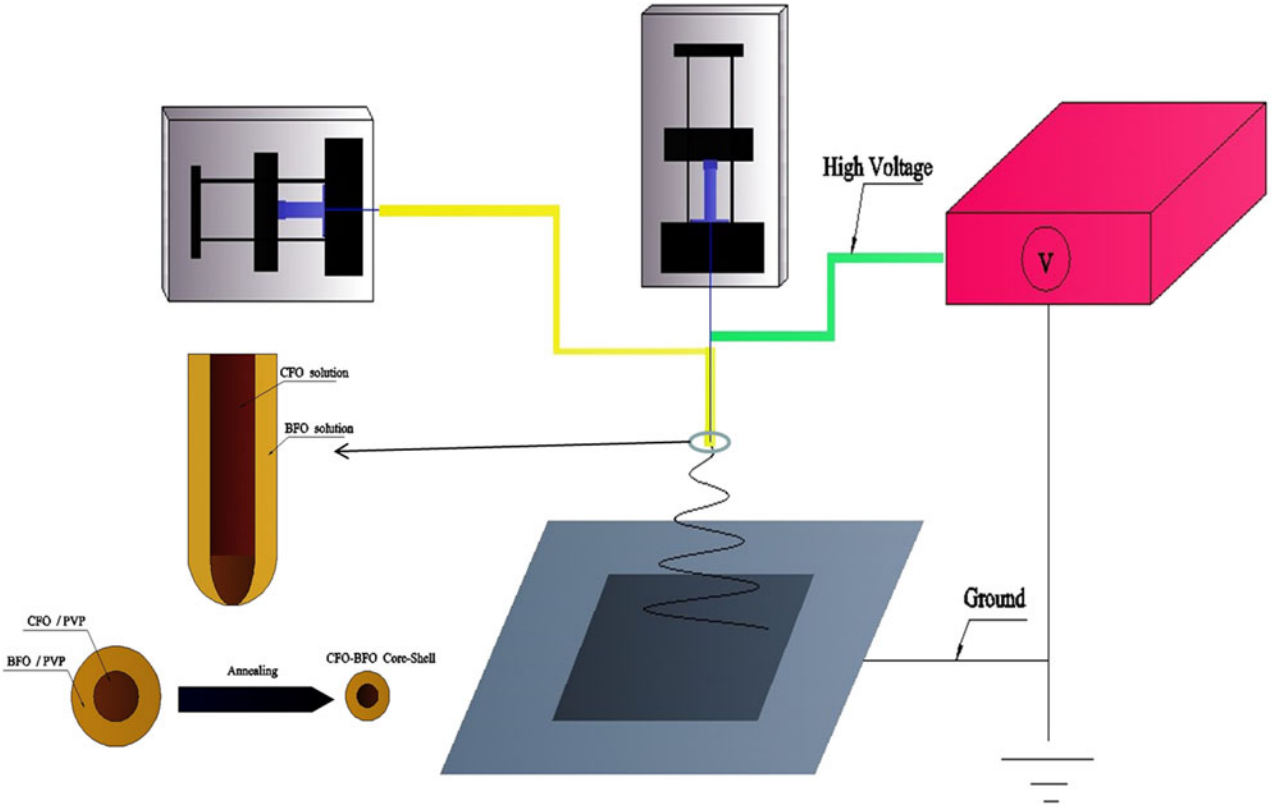


FIG. 1. The schematic setup of coaxial electrospinning system.

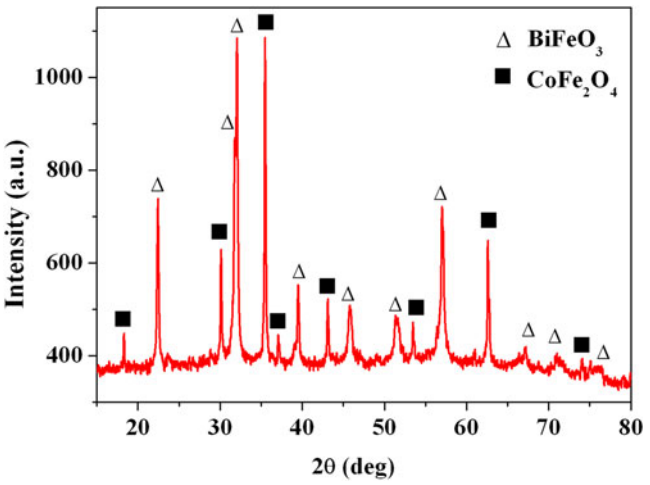


FIG. 2. XRD pattern of CFO–BFO core–shell nanofibers.

and XRD results. Both spinel structure of CFO and rhombohedral perovskite structure of BFO are confirmed by HRTEM in a single fiber, as shown in Fig. 3 (d), where the lattice space is measured to be 0.484 and 0.281 nm, corresponding to (111) plane of CFO phase and (012) plane of BFO phase, respectively. The interface between BFO shell and CFO core is compact without any gap, though it is not very sharp owing to the intermiscibility of BFO and CFO electrospinning solution, which is similar with previous work on PZT–CFO core–shell composite nanofibers.[28]

C. Ferromagnetic property

Room temperature ferromagnetism of the core–shell nanofibers was confirmed by magnetic hysteresis loop using VSM, as shown in Fig. 4. The remnant magnetization for the CFO–BFO core–shell nanofibers is measured to be 7.9 emu/g, which is larger than 4.0 emu/g while less than 31.8 emu/g that was measured from BFO and CFO nanofibers, respectively. The corresponding coercive field is measured to be around 650 Oe, between those of pure BFO and CFO nanofiber, which are 200 and 1700 Oe, respectively.[31,32]

D. Ferroelectric and ME coupling properties

The piezoelectricity of the core–shell nanofibers was examined by dual frequency PFM. Dual frequency resonance tracking technique is used for quantitative analysis, with the intrinsic vertical piezoresponse of the core shell fiber determined by correcting the quality factor Q,[33] as shown in Fig. 5. In addition, we apply an in-plane magnetic field to the core–shell nanofibers using VFM and examine the induced changes in PFM phase and amplitude as a mean to verify the ME coupling in the core–shell

https://doi.org/10.1557/jmr.2014.36 Published online by Cambridge University Press

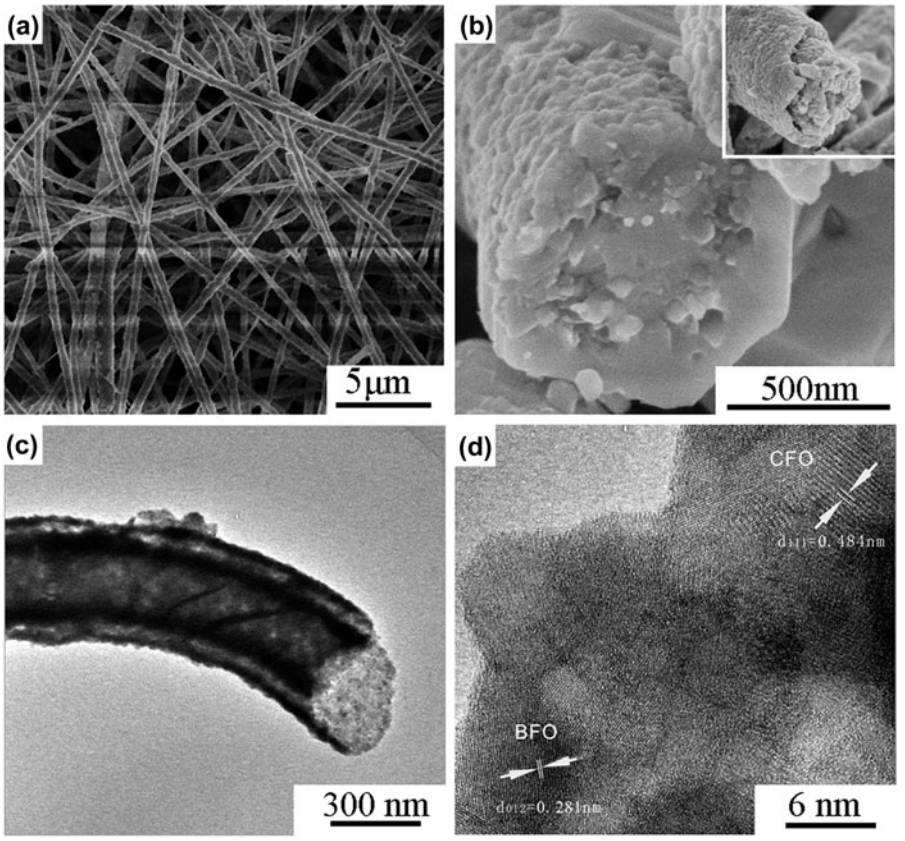


FIG. 3. The morphology and structure images of CFO–BFO core shell nanofibers: (a) SEM image of surface; (b) SEM image of cross section; (c) TEM; and (d) HRTEM images of typical nanofiber.

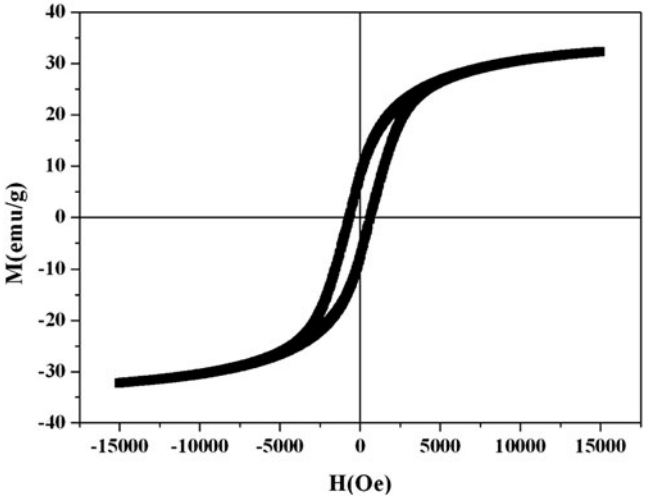


FIG. 4. VSM magnetic hysteresis loops of CFO–BFO core shell nanofibers.

nanofibers. Due to extremely small nanofiber cross-section, the ME coupling induced by the magnetic field is extremely small, making it very difficult to measure, and our PFM-based technique offers a convenient method to verify such ME coupling at nanoscale.[34] The diameter of the CFO core BFO shell nanofiber for PFM test in sample 1 is around 300 nm, while its height is less than 60 nm, as revealed by the topographic images in Figs. 5(a1) and 5(e1). The resulting PFM phase [Figs. 5(b1) and 5(f1)] mappings before and after the application of magnetic field are then obtained by measuring the piezoelectric vibration of the fiber induced by the electric field applied through the conductive scanning probe microscopy (SPM) tip. After the application of 2000 Oe in-plane external magnetic field, changes in PFM phase are observed, as seen in Fig. 5(f1), with some initially connected domains separated, and other primal dispersive domains connected together, suggesting ferroelectric domain switching in BFO shell induced by an external magnetic field. Such ferroelectric switching is induced indirectly through the mechanical interactions between CFO magnetostrictive and BFO piezoelectric strains.[35]

The intrinsic vertical PFM amplitude of the core shell nanofiber is in the range from 5 to 15 pm, as shown in Figs. 5(c1) and 5(g1), and subtle differences exist between the two amplitude mappings due to magnetic field effect. It is obvious that the marginal substrate has no piezoresponse, and the maximum intrinsic amplitude in the right fringe region of fiber is around 15 pm due to the presence of BFO shell, while amplitude at the left fringe and central region is mostly close to 0 pm probably

https://doi.org/10.1557/jmr.2014.36 Published online by Cambridge University Press

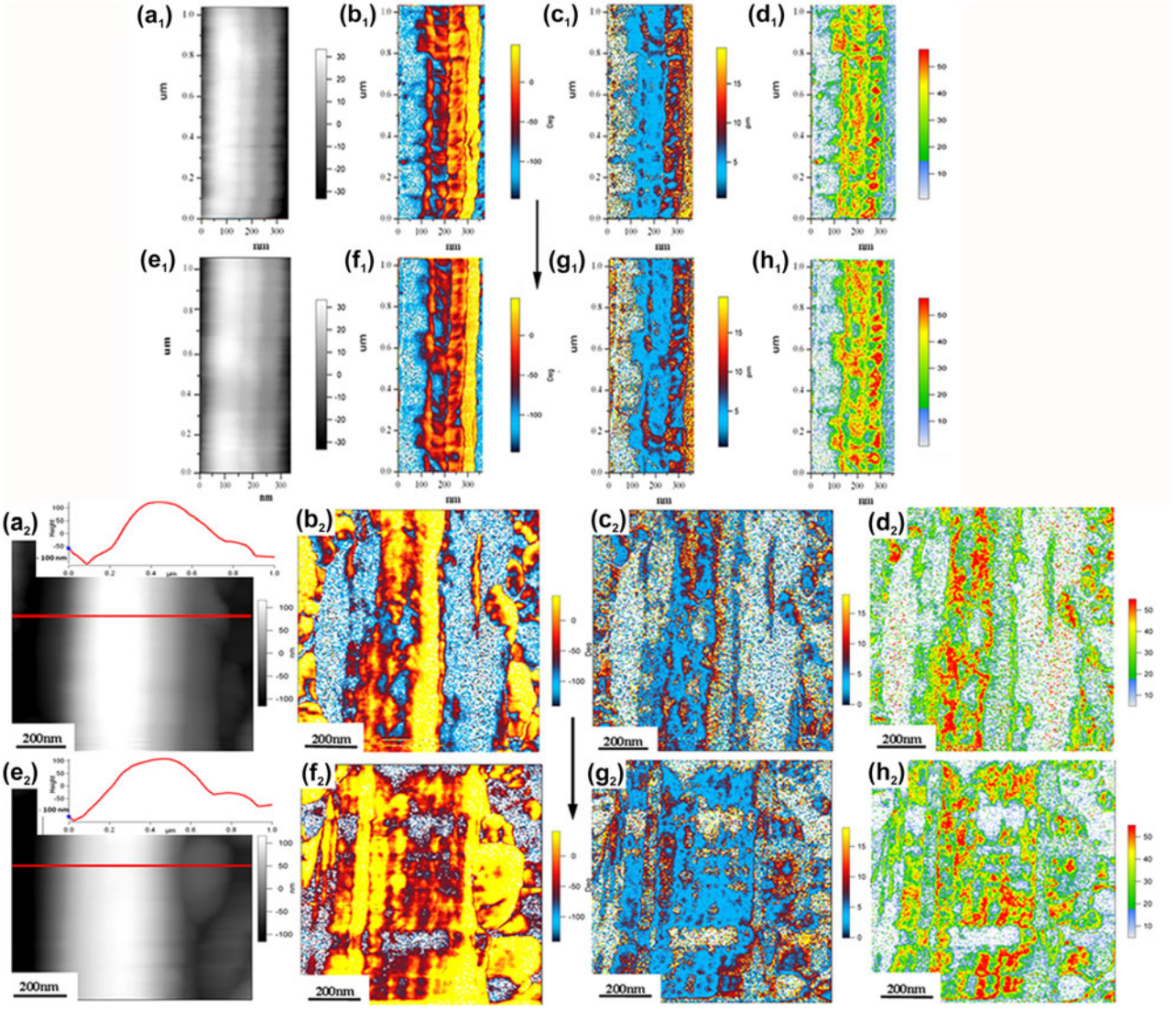


FIG. 5. The mapping of piezoresponse in the CFO–BFO core–shell nanofibers in two samples before and after the application of external magnetic field by VFM: (a_1) nanofiber topography, (a_2) topography with AFM height line scan across the fiber in the inset; (b_1), (b_2) PFM phase; (c_1), (c_2) intrinsic amplitude; and (d_1), (d_2) quality factor mapping without external magnetic field; (e_1) nanofiber topography, (e_2) topography with AFM height line scan across the fiber in the inset; (f_1), (f_2) PFM phase; (g_1), (g_2) intrinsic amplitude; and (h_1), (h_2) quality factor mapping under 2000 Oe; the direction of magnetic field is indicated by the arrow.

owing to the inhomogeneous phase diffusion between CFO core and BFO shell. The corresponding mappings of quality factor before and after the application of external magnetic field are shown in Figs. 5(d1) and 5(h1). The variation of quality factor Q in the nanofiber ranges between 20 and 50. When comparing Fig. 5(d1) with 5(h1) carefully, we found that the average quality factor is increased due to more obvious phase contrastive under magnetic field.

The vertical dual frequency PFM results of nanofiber in sample 2 were shown in Figs. 5(a2)–5(h2), and a corresponding morphology line scan is given in the inset of topography images. It is observed in Figs. 5(a2) and 5(e2) that the morphology of nanofiber changes a little under 2000 Oe magnetic field, and the negative magnetostrictive coefficient of CFO is confirmed from the AFM height line scan across the nanofiber, as demonstrated in the inset of Figs. 5(a2) and 5(e2), showing a small dilation in diameter direction and an observed left shift of the nanofiber, which indicates magnetostrictive strain change in the morphology of nanofiber subtly. Comparing Fig. 5(b2) with 5(f2), it is obvious that some domains switch, which confirms that the ferroelectric switching is induced through the strain-mediated magnetoelastic effect in CFO and piezoelectric effect in BFO. It is obvious that phase change in sample 2 is larger than sample 1 probably owing to having more compact interface structure. The intrinsic vertical PFM amplitude in

https://doi.org/10.1557/jmr.2014.36 Published online by Cambridge University Press

Figs. 5(c2) and 5(g2) is also low, which is consistent with the results of Figs. 5(c1) and 5(g1). The variation of quality factor Q in the sample 2 nanofiber is similar with that of sample 1.

The PFM amplitude–voltage butterfly loops and phase–voltage hysteresis loops are directly associated with the polarization switching of the CFO–BFO core–shell nanofibers. To further investigate the domain switching of the nanofibers, the piezoresponse hysteresis loops were measured at two different points both on the "OFF" states, as shown in Figs. 6(a) and 6(b). The OFF state means that the DC voltage is stepped back to zero. Measuring the loops in the OFF state is for minimizing the electrostatic interaction between tip and surface.[36] It is observed that in addition to PFM amplitude reduction as discussed earlier, the coercive field is increased by the applied magnetic field. Such trend is evident in the mappings of coercive voltage before and after the application of magnetic field, as shown in Figs. 6(c) and 6(d), where it is observed that the phase changes are about 180°, which proves domain switching of the nanofiber. The average coercive voltage is around 29.6 V in the absence of magnetic field, which increases to 34.4 V under 2000 Oe in point 1. This can be attributed to vertical compressive stress blocking the switching of ferroelectric polarization.[37,38] Similarly, the corresponding average coercive voltage is about 25.6 V and increased to 31.2 V under 2000 Oe in point 2. It is well known that the ME voltage coefficient $\alpha_E = dE/dH$, whereas for nanofiber it is very difficult to measure this coefficient directly. Here, we substitute dE with dE_C, estimating the ME coupling approximatively in nanoscale, where dE_C is the increased coercive field induced by an applied magnetic field dH. Then the strength of local ME interaction can be estimated as $dE/dH \approx 220$, 250 V/cm Oe for point 1 and point 2, respectively, which indicates that the ME response of nanofiber is different from point to point, common for nanomaterials. This local nanoscale ME coupling seems to be around one order of magnitude higher than multiferroic $CoFe_2O_4$–$Pb(Zr_{0.52}Ti_{0.48})O_3$ core shell nanofiber,[17] which is probably due to more compact interface. However, such local measurement cannot be compared with macroscopic ME coefficient directly.[39]

In summary, CFO–BFO core–shell nanofibers have been synthesized by coaxial electrospinning in combination with sol–gel process, and their microstructures have been thoroughly examined. Multiferroic properties of core–shell nanofibers have been verified, with their ferroelectricity confirmed by PFM mappings and switching characteristics, and ferromagnetism confirmed by VSM hysteresis. ME coupling of core–shell

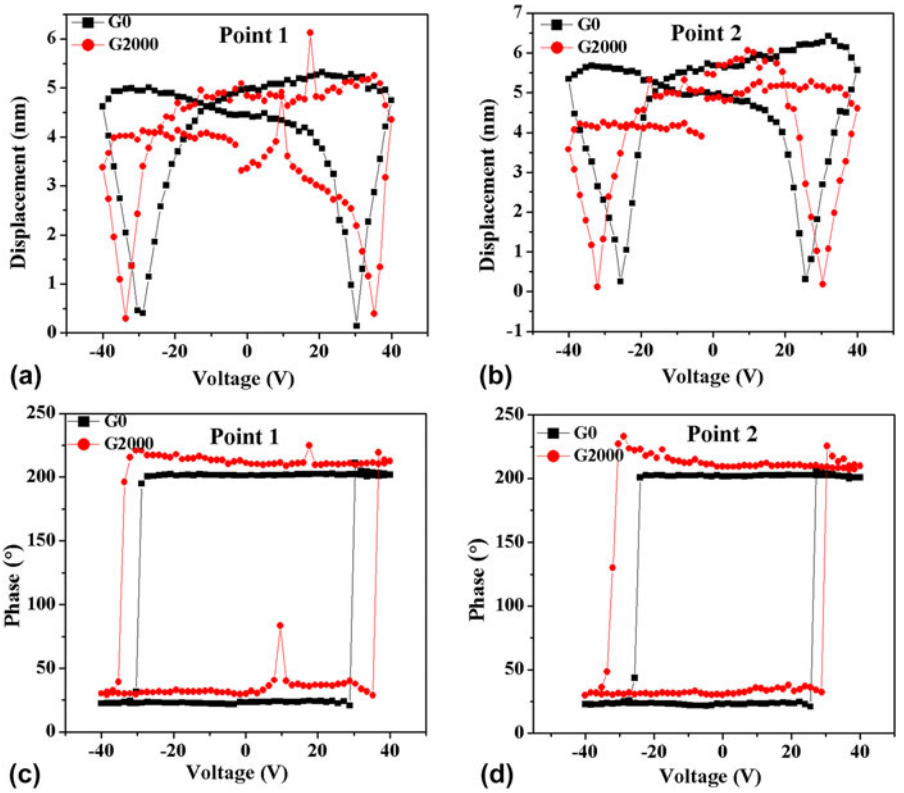


FIG. 6. PFM hysteresis loops of CFO–BFO core–shell nanofibers at two points before and after the application of external magnetic field: point 1 (a) and point 2 (b) of amplitude–voltage butterfly loop and point 1 (c) and point 2 (d) of phase–voltage hysteresis loop.

https://doi.org/10.1557/jmr.2014.36 Published online by Cambridge University Press

nanofibers has been observed using a novel SPM-based technique, with changes in PFM mapping and switching characteristics induced by an external magnetic field demonstrated. The nanofibers thus can find a variety of applications as one-dimensional multiferroic materials.

ACKNOWLEDGMENTS

We acknowledge the support of Natural Science Foundation of China (Approval Nos. 11372268, 11102175, and 51375017), and Provincial Natural Science Foundation of Hunan (13JJ1019).

REFERENCES

1. G. Smolenskiĭ and I. Chupis: Ferroelectromagnets. *Sov. Phys. Usp.* **25**, 475 (1982).
2. P. Dey, T. Nath, M.L. Nanda Goswami, and T. Kundu: Room temperature ferroelectric and ferromagnetic properties of multiferroics $xLa_{0.7}Sr_{0.3}MnO_3$-(1-x)$ErMnO_3$ (weight percent x=0.1, 0.2) composites. *Appl. Phys. Lett.* **90**, 162510 (2007).
3. C.W. Nan: Magnetoelectric effect in composites of piezoelectric and piezomagnetic phases. *Phys. Rev. B* **50**, 6082 (1994).
4. N.A. Spaldin and M. Fiebig: The renaissance of magnetoelectric multiferroics. *Science* **309**, 391 (2005).
5. N.A. Hill: Why are there so few magnetic ferroelectrics? *J. Phys. Chem. B* **104**, 6694 (2000).
6. N. Hur, S. Park, P. Sharma, J. Ahn, S. Guha, and S. Cheong: Electric polarization reversal and memory in a multiferroic material induced by magnetic fields. *Nature* **429**, 392 (2004).
7. L. Lin, Y. Wan, and F. Li: An analytical nonlinear model for laminate multiferroic composites reproducing the DC magnetic bias dependent magnetoelectric properties. *IEEE Trans. Ultrason. Ferroelectr. Freq. Control* **59**, 1568 (2012).
8. L. Li, J. Li, Y. Shu, and J. Yen: The magnetoelectric domains and cross-field switching in multiferroic $BiFeO_3$. *Appl. Phys. Lett.* **93**, 192506 (2008).
9. J. Ma, J. Hu, Z. Li, and C.W. Nan: Recent progress in multiferroic magnetoelectric composites: From bulk to thin films. *Adv. Mater.* **23**, 1062 (2011).
10. Y. Fetisov and G. Srinivasan: Electric field tuning characteristics of a ferrite-piezoelectric microwave resonator. *Appl. Phys. Lett.* **88**, 143503 (2006).
11. R. Ramesh and N.A. Spaldin: Multiferroics: Progress and prospects in thin films. *Nat. Mater.* **6**, 21 (2007).
12. C.W. Nan, M.I. Bichurin, S.X. Dong, D. Viehland, and G. Srinivasan: Multiferroic magnetoelectric composites: Historical perspective, status, and future directions. *J. Appl. Phys.* **103**, 031101 (2008).
13. J.P. Zhou, L. Lv, Q. Liu, Y.X. Zhang, and P. Liu: Hydrothermal synthesis and properties of $NiFe_2O_4$@$BaTiO_3$ composites with well-matched interface. *Sci. Technol. Adv. Mater.* **13**, 045001 (2012).
14. J.G. Wan, J.M. Liu, G.H. Wang, and C.W. Nan: Magnetoelectric $CoFe_2O_4$-lead zirconate titanate thick films prepared by a polyvinylpyrrolidone-assisted sol-gel method. *Appl. Phys. Lett.* **88**, 182502 (2006).
15. J.R. Hattrick-Simpers, L. Dai, M. Wuttig, I. Takeuchi, and E. Quandt: Demonstration of magnetoelectric scanning probe microscopy. *Rev. Sci. Instrum.* **78**, 106103 (2007).
16. C.L. Zhang, W.Q. Chen, S.H. Xie, J.S. Yang, and J.Y. Li: The magnetoelectric effects in multiferroic composite nanofibers. *Appl. Phys. Lett.* **94**, 102907 (2009).
17. S.H. Xie, F.Y. Ma, Y.M. Liu, and J.Y. Li: Multiferroic $CoFe_2O_4$-Pb$(Zr_{0.52}Ti_{0.48})O_3$ core-shell nanofibers and their magnetoelectric coupling. *Nanoscale* **3**, 3152 (2011).
18. R.J. Zeches, M.D. Rossell, J.X. Zhang, A.J. Hatt, Q. He, C.H. Yang, A. Kumar, C. H. Wang, A. Melville, C. Adamo, G. Sheng, Y.H. Chu, J.F. Ihlefeld, R. Erni, C. Ederer, V. Gopalan, L. Q. Chen, D.G. Schlom, N.A. Spaldin, L.W. Martin, and R. Ramesh: A strain-driven morphotropic phase boundary in $BiFeO_3$. *Science* **326**, 977 (2009).
19. Y. Lu, Y. Yin, Z.Y. Li, and Y. Xia: Synthesis and self-assembly of Au@SiO_2 core shell colloids. *Nano Lett.* **2**, 785 (2002).
20. M. Liu, X. Li, H. Imrane, Y. Chen, T. Goodrich, Z. Cai, K.S. Ziemer, J.Y. Huang, and N.X. Sun: Synthesis of ordered arrays of multiferroic $NiFe_2O_4$-Pb$(Zi_{0.52}Ti_{0.48})O_3$ core-shell nanowires. *Appl. Phys. Lett.* **90**, 152501 (2007).
21. X.M. Sun, J. Liu, and Y. Li: Oxides@C core-shell nanostructures: One-pot synthesis, rational conversion, and Li storage property. *Chem. Mater.* **18**, 3486 (2006).
22. L.J. Lauhon, M.S. Gudiksen, D. Wang, and C.M. Lieber: Epitaxial core-shell and core-multishell nanowire heterostructures. *Nature* **420**, 57 (2002).
23. Z.M. Huang, Y.Z. Zhang, M. Kotaki, and S. Ramakrishna: A review on polymer nanofibers by electrospinning and their applications in nanocomposites. *Compos. Sci. Technol.* **63**, 2223 (2003).
24. Z. Sun, E. Zussman, A.L. Yarin, J.H. Wendorff, and A. Greiner: Compound core–shell polymer nanofibers by co-electrospinning. *Adv. Mater.* **15**, 1929 (2003).
25. Y.Z. Zhang, Z.M. Huang, X.J. Xu, C.T. Lim, and S. Ramakrishna: Preparation of core-shell structured PCL-r-gelatin Bi-component nanofibers by coaxial electrospinning. *Chem. Mater.* **16**, 3406 (2004).
26. J.Y. Park, S.W. Choi, J.W. Lee, C. Lee, and S.S. Kim: Synthesis and gas sensing properties of TiO_2–ZnO core-shell nanofibers. *J. Am. Ceram. Soc.* **92**, 2551 (2009).
27. S.H. Xie, Y.Y. Liu, and J.Y. Li: Synthesis, microstructures, and magnetoelectric couplings of electrospun multiferroic nanofibers. *Front. Phys.* **4**, 399 (2012).
28. Y. Xie, Y. Ou, F.Y. Ma, X.L. Tan, and S.H. Xie: Synthesis of multiferroic Pb$(Zr_{0.52}Ti_{0.48})O_3$-$CoFe_2O_4$ core-shell nanofibers by coaxial electrospinning. *Nanosci. Nanotechnol. Lett.* **5**, 546 (2013).
29. Y.H. Hsieh, J.M. Liou, B.C. Huang, C.W. Liang, Q. He, Q. Zhan, Y.P. Chiu, Y.C. Chen, and Y.H. Chu: Local conduction at the $BiFeO_3$-$CoFe_2O_4$ tubular oxide interface. *Adv. Mater.* **24**, 4564 (2012).
30. X.L. Liu, M.Y. Li, J. Wang, Z.Q. Hu, Y.D. Zhu, and X.Z. Zhao: Preparation and characterization of multiferroic $CoFe_2O_4$/$Bi_{0.97}Ce_{0.03}FeO_3$ coaxial nanotubes. *Appl. Phys. A* **108**, 829 (2012).
31. S.H. Xie, J.Y. Li, R. Proksch, Y.M. Liu, Y.C. Zhou, Y.Y. Liu, Y. Ou, L.N. Lan, and Y. Qiao: Nanocrystalline multiferroic $BiFeO_3$ ultrafine fibers by sol-gel based electrospinning. *Appl. Phys. Lett.* **93**, 222904 (2008).
32. Y.W. Ju, J.H. Park, H.R. Jung, S.J. Cho, and W.J. Lee: Fabrication and characterization of cobalt ferrite ($CoFe_2O_4$) nanofibers by electrospinning. *Mater. Sci. Eng., B* **147**, 7 (2008).
33. B.J. Rodriguez, C. Callahan, S.V. Kalinin, and R. Proksch: Dual-frequency resonance-tracking atomic force microscopy. *Nanotechnology* **18**, 475504 (2007).
34. S.H. Xie, A. Gannepalli, Q.N. Chen, Y.M. Liu, Y.C. Zhou, R. Proksch, and J.Y. Li: High resolution quantitative piezoresponse force microscopy of $BiFeO_3$ nanofibers with dramatically enhanced sensitivity. *Nanoscale* **4**, 408 (2012).
35. F.X. Li and R.K.N.D. Rajapakse: A constrained domain-switching model for polycrystalline ferroelectric ceramics. Part II: Combined

https://doi.org/10.1557/jmr.2014.36 Published online by Cambridge University Press

switching and application to rhombohedral materials. *Acta Mater.* **55**, 6481 (2007).
36. S. Jesse, A.P. Baddorf, and S.V. Kalinin: Switching spectroscopy piezoresponse force microscopy of ferroelectric materials. *Appl. Phys. Lett.* **88**, 062908 (2006).
37. L. Lian and N.R. Sottos: Stress effects in sol-gel derived ferroelectric thin films. *J. Appl. Phys.* **95**, 629 (2004).
38. J.X. Zhang, J.Y. Dai, C.K. Chow, C.L. Sun, V.C. Lo, and H.L.W. Chan: Magnetoelectric coupling in $CoFe_2O_4/SrRuO_3/Pb(Zr_{0.52}Ti_{0.48})O_3$ heteroepitaxial thin film structure. *Appl. Phys. Lett.* **92**, 022901 (2008).
39. L. Yan, Z. Xing, Z. Wang, T. Wang, G. Lei, J. Li, and D. Viehland: Direct measurement of magnetoelectric exchange in self-assembled epitaxial $BiFeO_3$-$CoFe_2O_4$ nanocomposite thin films. *Appl. Phys. Lett.* **94**, 192902 (2009).

https://doi.org/10.1557/jmr.2014.36 Published online by Cambridge University Press